Atmos. Meas. Tech. Discuss., 6, 3611–3642, 2013
www.atmos-meas-tech-discuss.net/6/3611/2013/
doi:10.5194/amtd-6-3611-2013

Atmospheric Measurement Techniques Discussions

Retrieval of nitric oxide in the mesosphere and lower thermosphere with SCIAMACHY

S. Bender[1], M. Sinnhuber[1], J. P. Burrows[2], M. Langowski[2], B. Funke[3], and M. López-Puertas[3]

[1]Karlsruhe Institute of Technology, Karlsruhe, Germany
[2]University of Bremen, Bremen, Germany
[3]Instituto de Astrofísica de Andalucía, Granada, Spain

Received: 28 March 2013 – Accepted: 1 April 2013 – Published: 12 April 2013

Correspondence to: S. Bender (stefan.bender@kit.edu)

Published by Copernicus Publications on behalf of the European Geosciences Union.

Abstract

We use the ultra-violett (UV) spectra in the range 230–300 nm from the SCanning Imaging Absorption spectroMeter for Atmospheric CHartographY (SCIAMACHY) to retrieve the nitric oxide (NO) number densities from atmospheric emissions in the gamma-bands in the mesosphere and lower thermosphere. Using 3-D ray tracing, a 2-D retrieval grid, and regularisation with respect to altitude and latitude, we retrieve a whole semi-orbit simultaneously for the altitude range from 60 to 160 km.

We present details of the retrieval algorithm, first results, and initial comparisons to data from the Michelson Interferometer for Passive Atmospheric Sounding (MIPAS). Our results agree on average well with MIPAS data and are compatible with previously published measurements from other instruments. For the time of available measurements in 2008–2011, we achieve a vertical resolution of 5–10 km in the altitude range 70–140 km and a horizontal resolution of about 9° from 60° S–60° N. With this we have independent measurements of the NO densities in the mesosphere and lower thermosphere with approximately global coverage.

1 Introduction

Observations of a number of Antarctic and Arctic winters have shown that in polar regions, downwelling of nitric oxides (NO_x = N, NO, NO_2) from the upper mesosphere and lower thermosphere can provide a significant source of NO_x in the polar upper and middle stratosphere, see, for example, Siskind et al. (2000); Funke et al. (2005a); Randall et al. (2009). However, it is not clear whether the source of these NO_x intrusions is from auroral production in the lower thermosphere, or due to local production in the mesosphere by relativistic electrons, see, e.g. Callis et al. (1998); Sinnhuber et al. (2011, 2012). The measurements with SCIAMACHY are quantifying this important coupling between the sun and the upper atmosphere as it is the only instrument

AMTD
6, 3611–3642, 2013

with a good sensitivity, temporal resolution, and global coverage in the middle and upper mesosphere (70–90 km).

SCIAMACHY was proposed in the 1988 to fly on the then Polar Orbiting Earth Mission, POEM-1 of the European Space Agency, see Burrows et al. (1995) and references therein. SCIAMACHY was selected as a nationally funded contribution: its industrial development being funded by German Aerospace (then DARA and later DLR). Subsequently the Dutch space agency (then NIVR, later NSO) joined the SCIAMACHY agency consortium in Phase A and then Belgium in Phase B. The scientific objectives of SCIAMACHY comprise, beside the study of trace gases in the upper troposhere and stratosphere, the study of the upper atmosphere. Thus the measurement of UV and visible atmospheric emission by molecules and atoms and retrieval of vertical profiles of atmospheric constituents in the mesosphere were targeted. SCIAMACHY has several different measurement modes. The SCIAMACHY proposal envisaged two spectrometers making passive remote sensing solar and lunar occultation measurements, coupled with limb or nadir measurements of the upwelling radiation at the top of the atmosphere on the sunlit side of the orbit. In phase A and B SCIAMACHY was descoped to one instrument making solar lunar occultation and alternate limb and nadir measurements (Burrows et al., 1995; Bovensmann et al., 1999). As a result of data rate limitations on Envisat, the limb scanning mode of SCIAMACHY was restricted from −2 km to about 93 km. However, in order to probe the mesosphere and thermosphere, the mesosphere and lower thermosphere (MLT) measurements mode was adopted as an additional limb mode since 2008. This manuscript addresses studies using this measurements mode.

We use a part of SCIAMACHY's UV channel 1 (214–334 nm) to infer the NO number densities from atmospheric emissions of the gamma bands in the mesosphere and lower thermosphere. The gamma bands were already used in the retrieval of NO from rocket and satellite experiments. The rocket experiments (Cleary, 1986; Eparvier and Barth, 1992) have a very limited spatio-temporal coverage as they are restricted to single-day flights, in August 1982 (Cleary, 1986) and in March 1989 (Eparvier and

AMTD
6, 3611–3642, 2013

Barth, 1992) and to the area close to the starting location, Poker Flat, Alaska, in both cases.

Satellite measurements of nitric oxide were first done with the SBUV spectrometer on board the Nimbus 7 satellite by Frederick and Serafino (1985) in nadir geometry using the NO (1,4) gamma emission at 255 nm. Further previous satellite experiments using the NO gamma bands in the ultra-violet spectral range include the Student Nitric Oxide Explorer (SNOE, Barth et al., 2003) which measured nitric oxide in the thermosphere (97 to 150 km) from March 1998 until December 2003. Results are published until September 2000 and are used by the NOEM empirical model of nitric oxide in the MLT region (Marsh et al., 2004). The Ionospheric Spectroscopy and Atmospheric Chemistry (ISAAC, Minschwaner et al., 2004) satellite performed measurements at 80–200 km and results are published for November 1999–December 1999.

Measurements of NO in the mesosphere using microwaves were done by the Sub-Millimitre Radiometer (SMR) on board the Odin satellite. Infrared measurements were performed by the Optical Spectrograph and InfraRed Imaging System (OSIRIS) on board the Odin satellite which measured nighttime NO from NO_2 airglow emissions up to 100 km (Sheese et al., 2011). Further infrared instruments are the Atmospheric Chemistry Experiment Fourier transform spectrometer (ACE-FTS) (Kerzenmacher et al., 2008) and MIPAS also on the ENVISAT satellite. The MIPAS instrument measures the vibrational–rotational emission lines of NO with its infrared spectrometer directly (Funke et al., 2005b; Bermejo-Pantaleón et al., 2011). It shares the satellite with SCIAMACHY but is oriented to view in the opposite direction. This means that MIPAS samples the air at approximately the same tangent points but with a delay of about 50 min. With its special upper atmosphere (UA) mode which, however, is also not continuous, it provides another independent verification of our results.

This paper is organised as follows: we present some details about SCIAMACHY and its MLT mode in Sect. 2, Sect. 3 goes into detail about the NO gamma bands and the retrieval method. Finally, our results and the comparisons to MIPAS data and the NOEM model are shown in Sect. 4.

AMTD
6, 3611–3642, 2013

2 SCIAMACHY MLT mode

SCIAMACHY is a limb sounding experiment aboard the European ENVISAT satellite flying in a sun-synchronous orbit at approximately 800 km altitude since 2002 (Burrows et al., 1995; Bovensmann et al., 1999). The wavelength range of SCIAMACHY extends from UV to the near infrared (220–2380 nm). From July 2008 to April 2012, SCIAMACHY performed observations in the mesosphere and lower thermosphere (MLT, 50–150 km) regularly twice per month; this limb mesosphere-thermosphere state was coordinated with the MIPAS upper atmosphere (UA) mode once every 30 days.

The MLT mode sampled the mesosphere and lower thermosphere at 30 limb points from 50 to 150 km with a vertical spacing of about 3 km. The scans were scheduled in place of the usual nominal mode limb scans from 0 to 90 km, so that the rest of the measurements within the orbit sequence remained unchanged and there were around 20 limb scans along a semi-orbit. This compares well with the MIPAS measurement sequence, which collects limb scans every four to five degrees and its UA mode scans from 50 to 170 km.

The use of the NO gamma bands for the SCIAMACHY retrieval, where the first electronic state needs to be excited first, restricts the real measurements to times with available sunlight for this excitation. That means we can only retrieve the NO densities at daytime with SCIAMACHY. In contrast to that, the use of the infrared bands by MIPAS allows them to measure the NO densities at night-time as well. We take this into account when comparing the measured densities from both instruments.

3 Retrieval algorithm

Fitting the calculated NO emissivities to the calibrated measured spectra gives the slant column densities. These are used to retrieve vertical profiles of number densities using a constrained iterative least squares algorithm based on the work by Rodgers (1976) and which is similar to the one used in the retrieval of the MIPAS data

AMTD
6, 3611–3642, 2013

products (von Clarmann et al., 2003; Funke et al., 2005b). Further inputs are the high-resolution solar spectrum (Chance and Kurucz, 2010) and the temperature from the NRLMSISE-00 model (Picone et al., 2002) for the emissivity calculation, as well as the NOEM model (Marsh et al., 2004) as the a priori data for the retrieval.

3.1 NO gamma bands

The NO gamma bands result from the electronic transition of the NO molecule from the first excited state, $A^2\Sigma^+$, to the ground state $X^2\Pi$. The excitation happens by absorbing solar UV light, which restricts our retrieval to daytime nitric oxide, as discussed at the end of Sect. 2.

The various gamma bands have different advantages and disadvantages. The ones to the vibrational ground state of the electronic ground state, e.g. the (1, 0), (2, 0) transitions, have the advantage of having high emission rates and the disadvantage of self-absorption, see, for example, Eparvier and Barth (1992); Stevens (1995). This makes the atmosphere optically thick with respect to these bands and the emissivity depends on the total slant column density along the line of sight (Eparvier and Barth, 1992). In contrast to that, transitions to a different vibrational state, e.g. the (0, 1), (0, 2), or (1, 4) transitions, have a lower emissivity, but the probability of self-absorption is greatly reduced.

3.2 NO emissivity calculation

The emissivities of the NO gamma bands are calculated following Stevens and others (Eparvier and Barth, 1992; Stevens, 1995). The emission rate factors $g_{v'v''}$ for the transition from the vibrational state v' of the electronically excited state to the vibrational state v'' of the electronic ground state are given by the sums over all rotational emission factors $g_{j'j''}$ (see Eparvier and Barth, 1992 and references therein), which

AMTD
6, 3611–3642, 2013

are given by

$$g_{j'j''} = \frac{S(j'j'')}{2j'+1}\,\omega_{j'j''}\cdot\sum_{j=\|\Lambda+\Sigma\|}^{\infty}\frac{\pi e^2}{mc^2}\lambda_{j'j}^2\,\pi F_{j'j}f_{v'0}\frac{S(j'j)}{2j+1}\frac{N_j}{N_0}\,. \quad (1)$$

Here, S are the Hönl–London factors for the rotational transitions (Earls, 1935; Schadee, 1964; Tatum, 1967), ω is the branching fraction, λ the transition wavelength, πF the solar irradiance at that wavelength, and f the oscillator strength. More details and references for the actual values of these constants can be found in Eparvier and Barth (1992).

The calculated spectrum at 200 K for a selected number of gamma bands is shown in Fig. 1, where the small black lines indicate the individual rotational transitions and the larger envelope lines result from binning to the SCIAMACHY resolution and the convolution with the spectral slit function of the instrument. The spectra are calculated using spectroscopic data (oscillator strengths and branching fractions) from Luque and Crosley (1999).

The gamma bands shown in Fig. 1 are the ones that are visible in SCIAMACHY's UV channel 1. For the retrieval we use the three gamma bands with the largest emissivities in that spectral range, which are the (0,2), the (1,4), and the (1,5) bands at 247, 255, and 267 nm, respectively. These are all non-resonant bands and the line of sight should be optically thin.

The integrated band emission rate factors for 200 and 1000 K are listed in Table 1, with the top line listing the numbers used in previous work (Minschwaner et al., 2004) using the parameters from Piper and Cowles (1986); Stevens (1995). The emission rate factors used in this work are listed in the second line, calculated using the experimentally derived parameters from (Luque and Crosley, 1999). They agree within a few percent and the differences can be attributed to using slightly different oscillator strengths and branching fractions.

The variation of the emissivity over the temperature range from 200 to 1000 K is smaller than five percent, see Table 1. It is less for the temperature range found in

AMTD
6, 3611–3642, 2013

the thermosphere (200 . . . 600 K) such that the additional error induced by using model temperatures from NRLMSISE-00 (Picone et al., 2002) instead of the measured temperatures by MIPAS (Bermejo-Pantaleón et al., 2011), although deviations around thirty up to sixty percent from the model were found, is even smaller.

3.3 Radiative transfer

The general forward model is the functional relation

$$\boldsymbol{y} = F(\boldsymbol{x}) \tag{2}$$

between the measurements $\boldsymbol{y}$ and the quantities of interest $\boldsymbol{x}$. In the case discussed in this paper, the measurements are the spectral irradiances at the frequency ν (or at wavelength λ) at the satellite point, I_ν. Of interest are the number densities of NO at the retrieval point s, $\boldsymbol{x}(s)$.

The measured irradiance I_ν at the frequency ν is given by the radiative transfer equation as the integral over the line of sight

$$I_\nu = \int_{\mathrm{LOS}} (x(s)\gamma_\nu(s)F_{\nu'}(s) + \sigma_\mathrm{R}\varrho_\mathrm{air})\,\mathrm{e}^{-\tau_\nu}\mathrm{d}s \tag{3}$$

$$\approx \gamma F \int_{\mathrm{LOS}} x(s)\mathrm{d}s = \gamma F \cdot \varrho_\mathrm{sc}\,. \tag{4}$$

In Eq. (3), x is the number density of the species, γ the emissivity factor, and F the solar irradiance at the excitation frequency ν'. The Rayleigh part of the spectrum, $\sigma_\mathrm{R}\varrho_\mathrm{air}$, is fitted as a spectral background signal. Since we use non-resonant transitions, the line of sight is optically thin, i.e. the self-absorption is negligible and the optical path length is mainly determined by the ozone and air absorption along the line of sight and the line from the sun. This absorption is taken into account by adjusting the emissivity, leaving us with the linear relationship of the intensity to the slant column density ϱ_sc in Eq. (4).

AMTD
6, 3611–3642, 2013

3.4 Retrieval algorithm

The general problem is to invert Eq. (2) to extract $\boldsymbol{x}$ from $\boldsymbol{y}$, where there are usually a different number of measurements ($\boldsymbol{y}$) than unknowns ($\boldsymbol{x}$), which means that Eq. (2) is underdetermined or overdetermined. In the case of an overdetermined system, this inversion problem can be solved by minimising

$$\|\mathbf{K}\boldsymbol{x} - \boldsymbol{y}\|^2 , \tag{5}$$

where $\mathbf{K}$ is the Jacobian of the forward model Eq. (2). In our case, the measurements $\boldsymbol{y}$ are the slant column densities deduced from fitting the calculated NO spectra to the measured ones.

In the case of an underdetermined system, additional constraints are needed. These are given by the a priori input, i.e. approximate knowledge of the solution $\boldsymbol{x}$. The minimisation problem then changes to

$$\|\mathbf{K}\boldsymbol{x} - \boldsymbol{y}\|^2_{\mathbf{S}_y^{-1}} + \|\boldsymbol{x} - \boldsymbol{x}_\mathrm{a}\|^2_{\mathbf{S}_\mathrm{a}^{-1}} , \tag{6}$$

where $\mathbf{S}$ are the covariance matrices and the subscript "a" indicates the a priori quantities. Doing a 2-D-retrieval, we additionally constrain the solutions to not vary too much with altitude and latitude by introducing regularisation matrices $\mathbf{R}_\mathrm{alt}$ and $\mathbf{R}_\mathrm{lat}$, see Scharringhausen et al. (2008a). This then leads to the minimisation of

$$\|\mathbf{K}\boldsymbol{x} - \boldsymbol{y}\|^2_{\mathbf{S}_y^{-1}} + \|\boldsymbol{x} - \boldsymbol{x}_\mathrm{a}\|^2_{\mathbf{S}_\mathrm{a}^{-1}} + \lambda_\mathrm{alt}\|\mathbf{R}_\mathrm{alt}(\boldsymbol{x} - \boldsymbol{x}_\mathrm{a})\|^2 + \lambda_\mathrm{lat}\|\mathbf{R}_\mathrm{lat}(\boldsymbol{x} - \boldsymbol{x}_\mathrm{a})\|^2 \tag{7}$$

in our case.

The solution of Eq. (7) is obtained by an iterative algorithm. Defining a combined regularisation matrix $\mathbf{R}$ as

$$\mathbf{R} := \mathbf{S}_\mathrm{a}^{-1} + \lambda_\mathrm{alt}\mathbf{R}_\mathrm{alt}^T\mathbf{R}_\mathrm{alt} + \lambda_\mathrm{lat}\mathbf{R}_\mathrm{lat}^T\mathbf{R}_\mathrm{lat} , \tag{8}$$

the intermediate solution is given by (von Clarmann et al., 2003; Funke et al., 2005b)

$$\boldsymbol{x}_{i+1} = \boldsymbol{x}_i + \left(\mathbf{K}^T\mathbf{S}_y^{-1}\mathbf{K} + \mathbf{R}\right)^{-1} \cdot \left[\mathbf{K}^T\mathbf{S}_y^{-1}(\boldsymbol{y} - \boldsymbol{y}_i(\boldsymbol{x}_i)) + \mathbf{R}(\boldsymbol{x}_\mathrm{a} - \boldsymbol{x}_i)\right] . \tag{9}$$

AMTD
6, 3611–3642, 2013

3.5 Model input

Our retrieval uses model input to provide an initial guess for the number density and to improve the convergence of the iteration. The a priori input stems from the NOEM model (Marsh et al., 2004), which is also used by the MIPAS NO retrievals (Funke et al., 2005b); it is an empirical model based on SNOE observations (Barth et al., 2003). It turns out that the use of the NOEM model for altitudes below 100 km is questionable, but it is used because of our comparisons to the MIPAS results, which use the same a priori input for the retrieval.

Another input necessary for the emissivity calculation of the NO rotational transitions are the atmospheric temperatures. These are calculated using the NRLMSISE-00 model (Picone et al., 2002), and has as additional input parameters the geomagnetic A_p index and the solar radio flux $f_{10.7}$. These data were taken from the Space Physics Interactive Data Resource (SPIDR) service (NGDC and NOAA, 2011) of the National Geophysical Data Center (NGDC) of the National Oceanic and Atmospheric Administration (NOAA).

4 Results

4.1 NO number density

To illustrate the results of our retrieval, we choose one example orbit, 41467 from 3 February 2010, to show the individual steps. For one selected tangent point, 71° N, 105 km, the spectral fit for the NO (0,2) transition is shown in Fig. 2. This latitude and altitude were chosen such that the NO content in that region is supposed to be non-negligible as indicated by previous measurements from SNOE (Barth et al., 2003). As the figure shows, the UV spectra can be noisy, i.e. the NO signal is near the noise threshold, introducing errors into the fitted slant column densities and reducing the signal-to-noise ratio (SNR). These errors are taken into account by the retrieval

AMTD
6, 3611–3642, 2013

algorithm as the covariance matrix $\mathbf{S}_y$, see Eqs. (6) and (7), giving less weight to points with a low SNR.

The resulting slant column densities for the same orbit are shown in Fig. 3 for the (0,2) transition. The largest slant column densities for all three lines (the other two are not shown here) are observed at approximately the same tangent points, namely in the region from 60° N–70° N and at altitudes around 100 km.

The zonal mean (60° N–90° N) for the line of sight emissivities are shown in the left panel of Fig. 4. They are obtained by integrating the relevant part of the measured spectrum and averaging the results with equal weights. The maximum of the emissivity profile is observed slightly below 100 km limb tangent altitude. The profile of the fitted slant column densities, shown in the middle panel of the same figure, shows the same features and reflects the measured emissivities. The resulting number density profile is shown in the right panel of Fig. 4. It shows that the altitude of the largest number density is above the peak emissivity and peak slant column density. This is the result of the retrieval algorithm that takes into account that the slant column density is given by the total NO emission along the line of sight which is largest at a tangent point where the line of sight includes the whole NO layer in the thermosphere, i.e. slightly below 100 km.

Using the retrieval algorithm as described in Sect. 3, the calculated number density distribution along the orbit is shown in Fig. 5. As already indicated by the slant column densities and the number density profile in Fig. 4, the maximum here is between 60° N and 70° N and at an altitude of around 100–110 km. In the northern winter there is polar night at latitudes north of 80°, hence the retrieval of NO in this region is not possible.

4.2 Resolution

To assess the quality of the results, the vertical averaging kernel elements of our retrieval of that particular orbit are shown in Fig. 6 with the respective full width at half maximum (fwhm) resolution shown in Fig. 7. The vertical resolution is 10 km or better in the range from 70 to 150 km and we achieve about 5 km resolution from 80 to 140 km.

AMTD
6, 3611–3642, 2013

The horizontal averaging kernel elements for the same orbit are presented in Fig. 8 with the respective fwhm shown in Fig. 9. The horizontal resolution is quite constant between 60° S and 60° N, around 9°.

4.3 Number density time series

For the time of available MLT spectra from July 2008 until March 2011, the NO number density at 106 km in the equatorial region (5° S–5° N) is shown in Fig. 10, and for the auroral region (60° N–66° N) in Fig. 11. We compare our results to MIPAS UA data and to the NOEM model (Marsh et al., 2004) which is derived from SNOE measurements (Barth et al., 2003).

SCIAMACHY and NOEM agree reasonably well in both geographic regions, where they are of the same order of magnitude. However, the NOEM results are systematically higher than the SCIAMACHY data. This disagreement is largest in 2008 and 2009, during the deep solar minimum, when also the geomagnetic activity was very low; in 2010, when both solar and geomagnetic activity were beginning to increase again, the agreement is better. Nearly perfect agreement is reached in 2011 at high latitudes. The consistency among the MIPAS and SCIAMACHY data may hint at a problem with the NOEM model which was derived from SNOE observations during a period of continuous high solar and geomagnetic activity (1998–2000).

4.4 Comparison to MIPAS measurements

Since MIPAS and SCIAMACHY share the same satellite, although viewing in the opposite direction, a direct comparison of the results is desirable. Data products from the MIPAS instrument (Bermejo-Pantaleón et al., 2011) include the volume mixing ratio (vmr) rather than the number densities of NO. We have converted the MIPAS vmr values to number densities using their retrieved temperatures and compare the vertical columns in the range of 70–140 km to the SCIAMACHY derived results. For a meaningful comparison, the vertical column ratios (SCIAMACHY/MIPAS) for orbits where

AMTD
6, 3611–3642, 2013

both instruments scanned the upper atmosphere are binned into 20° latitude bins and are shown for 2008 in Fig. 12 and for 2009 in Fig. 13. The MIPAS measurements are thereby restricted to daylight limb scans, selected by the requirement that the solar zenith angle must be smaller than 95°, since the comparison goes down to 70 km.

Another fact is the different latitude spacing of the limb scans, SCIAMACHY has about 6° distance between two consecutive scans and MIPAS has 4–5°. This means that there are around three SCIAMACHY limb scans in a 20° bin, and four to five MIPAS limb scans, affecting the statistics slightly.

The ratio is compatible with one considering the standard deviation of the bin means (error bars). We find that our SCIAMACHY results are almost always a bit above the MIPAS results, except for higher northern latitudes (in particular in 2008), where there are not many simultaneous measurements. Here, the SCIAMACHY retrieval attempts to reproduce the absolute number densities of the a priori information (NOEM model), while the MIPAS retrieval is oriented on the density changes provided by the model.

5 Conclusions

We present a retrieval algorithm for the extraction of NO number densities in the mesosphere and lower thermosphere (MLT) region with the SCIAMACHY instrument aboard ENVISAT. The method is adapted from earlier work (cf. Scharringhausen et al. (2008b,a)) and was extended to use the gamma bands of NO and the UV spectra of SCIAMACHY's special MLT limb scans. The retrieval method is an adapted version of the MIPAS retrieval algorithm to be found in von Clarmann et al. (2003); Funke et al. (2005b) and using 3-D ray tracing, a 2-D retrieval grid, and regularisation with respect to altitude and latitude allows us to retrieve a whole semi-orbit at once for the altitude range from 60–160 km.

We find that the retrieval of NO number densities from the fit of calculated spectra for the NO gamma bands gives very usable results which are compatible with previous measurements from Barth et al. (2003); Minschwaner et al. (2004). A first comparison

AMTD
6, 3611–3642, 2013

shows that they are also in good agreement with the measurements of the MIPAS instrument on board the same satellite for the orbits where both instruments scanned the upper atmosphere (50–150 km). For low geomagnetic activity (low A_p) in 2008–2010, we obtain a vertical resolution of 5–10 km in the altitude range 70–150 km and a horizontal resolution of about 9°.

The current approach is successful in retrieving the NO number densities in the mesosphere and lower thermosphere with SCIAMACHY MLT limb scans. The results are in good agreement with previous measurements from other instruments and provide an almost continuous data source for NO in that region from 2008 to 2012. The latitudinal and longitudinal resolution might be further improved by using two-dimensional detector arrays, or they might provide a way for longer integration times in the case of weak signals,

Continuous measurements in that region over a long time span help to understand the connection between solar activity and thermospheric NO. Observations in the middle atmosphere then also allow to follow the NO produced from solar particles in the region around 100 km downwards during the polar winter, in particular during extraordinary atmospheric events such as stratospheric warmings. It also helps to disentangle anthropogenic influences on the atmospheric composition from the changes due to the varying solar activity during a solar cycle.

Acknowledgements. S. B. and M. S. thank the Helmholtz-society for funding this project under the grant number VH-NG-624. The SCIAMACHY project was funded by German Aerospace (DLR), the Dutch Space Agency, SNO, and the Belgium ministry. ESA funded the ENVISAT project. The University of Bremen as Principal Investigator has led the scientific support and development of SCIAMACHY and the scientific exploitation of its data products.

The service charges for this open access publication have been covered by a Research Centre of the Helmholtz Association.

References

Barth, C. A., Mankoff, K. D., Bailey, S. M., and Solomon, S. C.: Global observations of nitric oxide in the thermosphere, J. Geophys. Res., 108, 1027, doi:10.1029/2002JA009458, 2003. 3614, 3620, 3622, 3623, 3639, 3640

Bermejo-Pantaleón, D., Funke, B., López-Puertas, M., García-Comas, M., Stiller, G. P., von Clarmann, T., Linden, A., Grabowski, U., Höpfner, M., Kiefer, M., Glatthor, N., Kellmann, S., and Lu, G.: Global observations of thermospheric temperature and nitric oxide from MIPAS spectra at 5.3 µm, J. Geophys. Res., 116, A10313, doi:10.1029/2011JA016752, 2011. 3614, 3618, 3622

Bovensmann, H., Burrows, J. P., Buchwitz, M., Frerick, J., Noël, S., Rozanov, V. V., Chance, K. V., and Goede, A. P. H.: SCIAMACHY: Mission Objectives and Measurement Modes, J. Atmos. Sci., 56, 127–150, doi:10.1175/1520-0469(1999)056¡0127:SMOAMM¿2.0.CO;2, 1999. 3613, 3615

Burrows, J. P., Hölzle, E., Goede, A. P. H., Visser, H., and Fricke, W.: SCIAMACHY–scanning imaging absorption spectrometer for atmospheric chartography, Acta Astronaut., 35, 445–451, doi:10.1016/0094-5765(94)00278-T, 1995. 3613, 3615

Callis, L. B., Natarajan, M., Evans, D. S., and Lambeth, J. D.: Solar atmospheric coupling by electrons (SOLACE): 1. Effects of the May 12, 1997 solar event on the middle atmosphere, J. Geophys. Res., 103, 28405–28419, doi:10.1029/98JD02408, 1998. 3612

Chance, K. and Kurucz, R.: An improved high-resolution solar reference spectrum for earth's atmosphere measurements in the ultraviolet, visible, and near infrared, J. Quant. Spectrosc. Ra., 111, 1289–1295, doi:10.1016/j.jqsrt.2010.01.036, 2010. 3616

Cleary, D. D.: Daytime High-Latitude Rocket Observations of the NO γ, δ, and ε Bands, J. Geophys. Res., 91, 11337–11344, doi:10.1029/JA091iA10p11337, 1986. 3613

Earls, L. T.: Intensities in $^2\Pi - ^2\Sigma$ Transitions in Diatomic Molecules, Phys. Rev., 48, 423–424, doi:10.1103/PhysRev.48.423, 1935. 3617

Eparvier, F. G. and Barth, C. A.: Self-Absorption Theory Applied to Rocket Measurements of the Nitric Oxide (1, 0) γ Band in the Daytime Thermosphere, J. Geophys. Res., 97, 13723–13731, doi:10.1029/92JA00993, 1992. 3613, 3616, 3617

Frederick, J. E. and Serafino, G. N.: Satellite observations of the nitric oxide dayglow: Implications for the behavior of mesospheric and lower-thermospheric odd nitrogen, J. Geophys. Res., 90, 3821–3830, doi:10.1029/JD090iD02p03821, 1985. 3614

AMTD
6, 3611–3642, 2013

Funke, B., López-Puertas, M., Gil-López, S., von Clarmann, T., Stiller, G. P., Fischer, H., and Kellmann, S.: Downward transport of upper atmospheric NO_x into the polar stratosphere and lower mesosphere during the Antarctic 2003 and Arctic 2002/2003 winters, J. Geophys. Res., 110, D24308, doi:10.1029/2005JD006463, 2005a. 3612

Funke, B., López-Puertas, M., von Clarmann, T., Stiller, G. P., Fischer, H., Glatthor, N., Grabowski, U., Höpfner, M., Kellmann, S., Kiefer, M., Linden, A., Mengistu Tsidu, G., Milz, M., Steck, T., and Wang, D. Y.: Retrieval of stratospheric NO_x from 5.3 and 6.2 µm nonlocal thermodynamic equilibrium emissions measured by Michelson Interferometer for Passive Atmospheric Sounding (MIPAS) on Envisat, J. Geophys. Res., 110, D09302, doi:10.1029/2004JD005225, 2005b. 3614, 3616, 3619, 3620, 3623

Kerzenmacher, T., Wolff, M. A., Strong, K., Dupuy, E., Walker, K. A., Amekudzi, L. K., Batchelor, R. L., Bernath, P. F., Berthet, G., Blumenstock, T., Boone, C. D., Bramstedt, K., Brogniez, C., Brohede, S., Burrows, J. P., Catoire, V., Dodion, J., Drummond, J. R., Dufour, D. G., Funke, B., Fussen, D., Goutail, F., Griffith, D. W. T., Haley, C. S., Hendrick, F., Höpfner, M., Huret, N., Jones, N., Kar, J., Kramer, I., Llewellyn, E. J., López-Puertas, M., Manney, G., McElroy, C. T., McLinden, C. A., Melo, S., Mikuteit, S., Murtagh, D., Nichitiu, F., Notholt, J., Nowlan, C., Piccolo, C., Pommereau, J.-P., Randall, C., Raspollini, P., Ridolfi, M., Richter, A., Schneider, M., Schrems, O., Silicani, M., Stiller, G. P., Taylor, J., Tétard, C., Toohey, M., Vanhellemont, F., Warneke, T., Zawodny, J. M., and Zou, J.: Validation of NO_2 and NO from the Atmospheric Chemistry Experiment (ACE), Atmos. Chem. Phys., 8, 5801–5841, doi:10.5194/acp-8-5801-2008, 2008. 3614

Luque, J. and Crosley, D. R.: Transition probabilities and electronic transition moments of the $A^2\Sigma^+$–$X^2\Pi$ and $D^2\Sigma^+$–$X^2\Pi$ systems of nitric oxide, J. Chem. Phys., 111, 7405–7415, doi:10.1063/1.480064, 1999. 3617, 3629

Marsh, D. R., Solomon, S. C., and Reynolds, A. E.: Empirical model of nitric oxide in the lower thermosphere, J. Geophys. Res., 109, A07301, doi:10.1029/2003JA010199, 2004. 3614, 3616, 3620, 3622, 3639, 3640

Minschwaner, K., Bishop, J., Budzien, S. A., Dymond, K. F., Siskind, D. E., Stevens, M. H., and McCoy, R. P.: Middle and upper thermospheric odd nitrogen: 2. Measurements of nitric oxide from Ionospheric Spectroscopy and Atmospheric Chemistry (ISAAC) satellite observations of NO γ band emission, J. Geophys. Res., 109, A01304, doi:10.1029/2003JA009941, 2004. 3614, 3617, 3623, 3629

AMTD
6, 3611–3642, 2013

NGDC and NOAA: Space Physics Interactive Data Resource (SPIDR), available at: http://spidr.ngdc.noaa.gov/spidr/ (last access: 17 February 2012), 2011. 3620

Picone, J. M., Hedin, A. E., Drob, D. P., and Aikin, A. C.: NRLMSISE-00 empirical model of the atmosphere: Statistical comparisons and scientific issues, J. Geophys. Res., 107, 1468, doi:10.1029/2002JA009430, 2002. 3616, 3618, 3620

Piper, L. G. and Cowles, L. M.: Einstein coefficients and transition moment variation for the NO($A^2\Sigma^+$–$X^2\Pi$) transition, J. Chem. Phys., 85, 2419–2422, doi:10.1063/1.451098, 1986. 3617, 3629

Randall, C. E., Harvey, V. L., Siskind, D. E., France, J., Bernath, P. F., Boone, C. D., and Walker, K. A.: NO_x descent in the Arctic middle atmosphere in early 2009, Geophys. Res. Lett., 36, L18811, doi:10.1029/2009GL039706, 2009. 3612

Rodgers, C. D.: Retrieval of atmospheric temperature and composition from remote measurements of thermal radiation, Rev. Geophys., 14, 609–624, doi:10.1029/RG014i004p00609, 1976. 3615

Schadee, A.: The formation of molecular lines in the solar spectrum (Errata: 17 537), Bull. Astron. Inst. Neth., 17, 311–357, 1964. 3617

Scharringhausen, M., Aikin, A. C., Burrows, J. P., and Sinnhuber, M.: Global column density retrievals of mesospheric and thermospheric MgI and MgII from SCIAMACHY limb and nadir radiance data, J. Geophys. Res.-Atmos., 113, D13303, doi:10.1029/2007JD009043, 2008a. 3619, 3623

Scharringhausen, M., Aikin, A. C., Burrows, J. P., and Sinnhuber, M.: Space-borne measurements of mesospheric magnesium species – a retrieval algorithm and preliminary profiles, Atmos. Chem. Phys., 8, 1963–1983, doi:10.5194/acp-8-1963-2008, 2008b. 3623

Sheese, P. E., Gattinger, R. L., Llewellyn, E. J., Boone, C. D., and Strong, K.: Nighttime nitric oxide densities in the Southern Hemisphere mesosphere–lower thermosphere, Geophys. Res. Lett., 38, L15812, doi:10.1029/2011GL048054, 2011. 3614

Sinnhuber, M., Kazeminejad, S., and Wissing, J. M.: Interannual variation of NOx from the lower thermosphere to the upper stratosphere in the years 1991–2005, J. Geophys. Res.: Space Phys., 116, A02312, doi:10.1029/2010JA015825, 2011. 3612

Sinnhuber, M., Nieder, H., and Wieters, N.: Energetic Particle Precipitation and the Chemistry of the Mesosphere/Lower Thermosphere, Surv. Geophys., 33, 1281–1334, doi:10.1007/s10712-012-9201-3, 2012. 3612

AMTD
6, 3611–3642, 2013

Siskind, D. E., Nedoluha, G. E., Randall, C. E., Fromm, M., and Russell, J. M.: An assessment of southern hemisphere stratospheric NOx enhancements due to transport from the upper atmosphere, Geophys. Res. Lett., 27, 329–332, doi:10.1029/1999GL010940, 2000. 3612

Stevens, M. H.: Nitric Oxide γ Band Fluorescent Scattering and Self-Absorption in the Mesosphere and Lower Thermosphere, J. Geophys. Res., 100, 14735–14742, doi:10.1029/95JA01616,, 1995. 3616, 3617, 3629

Tatum, J. B.: The Interpretation of Intensities in Diatomic Molecular Spectra, Astrophys. J. Suppl., 14, 21–55, 1967. 3617

von Clarmann, T., Glatthor, N., Grabowski, U., Höpfner, M., Kellmann, S., Kiefer, M., Linden, A., Tsidu, G. M., Milz, M., Steck, T., Stiller, G. P., Wang, D. Y., Fischer, H., Funke, B., Gil-López, S., and López-Puertas, M.: Retrieval of temperature and tangent altitude pointing from limb emission spectra recorded from space by the Michelson Interferometer for Passive Atmospheric Sounding (MIPAS), J. Geophys. Res., 108, 4736, doi:10.1029/2003JD003602, 2003. 3616, 3619, 3623

AMTD
6, 3611–3642, 2013

Table 1. NO band integrated emission rate factors (in 10^{-6} ph s^{-1}) at 200 and 1000 K for the γ bands used in the retrieval. Top row: results from Stevens (1995), using the parameters from Piper and Cowles (1986), and used for NO retrieval by Minschwaner et al. (2004). Bottom row: factors used in this work, using the parameters from Luque and Crosley (1999).

Reference	T [K]	(0, 2)	(1, 4)	(1, 5)
Minschwaner et al. (2004) (cf. Stevens, 1995)	200	2.08	1.56	1.49
	1000	2.17	1.53	1.45
this work	200	2.02	1.60	1.39
	1000	2.11	1.57	1.37

AMTD
6, 3611–3642, 2013

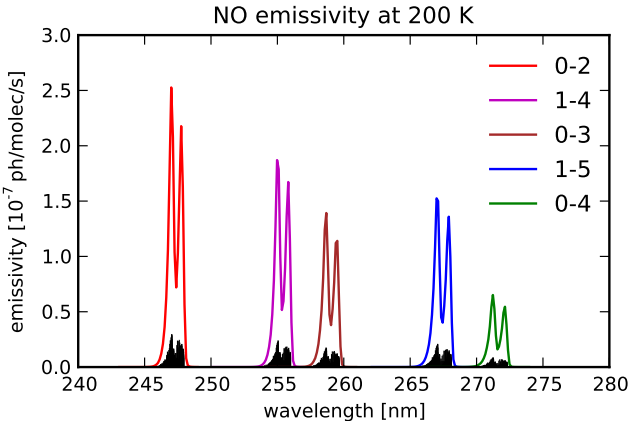

Fig. 1. NO emissivities calculated for a temperature of 200 K for a selected number of gamma bands. The small black lines indicate the individual rotational emission lines within the vibrational transition bands and the coloured lines are the emissivity bands resulting from binning to the SCIAMACHY spectral resolution and convolving with the respective spectral slit function.

AMTD
6, 3611–3642, 2013

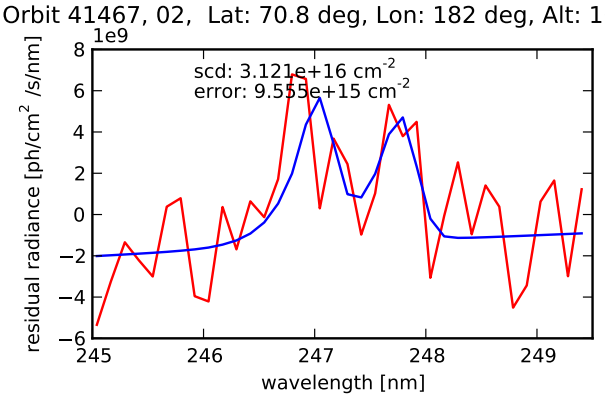

Fig. 2. NO (0,2) spectral fit, showing the residual spectra (red) after dark-current subtraction and Rayleigh background fit, and the fitted NO spectrum (blue) with a low order polynomial as a baseline.

AMTD
6, 3611–3642, 2013

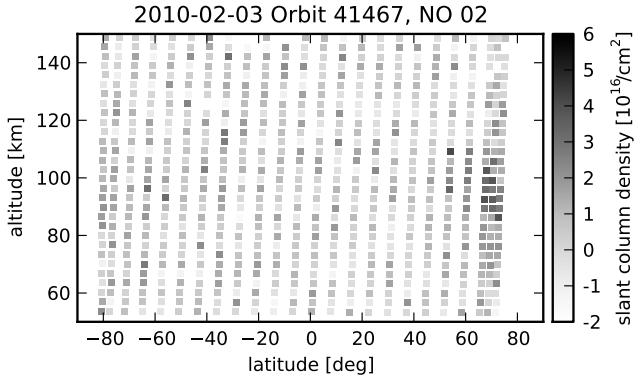

Fig. 3. NO slant column densities for the (0,2) transition along the sample orbit (no. 41467, 3 February 2010).

AMTD
6, 3611–3642, 2013

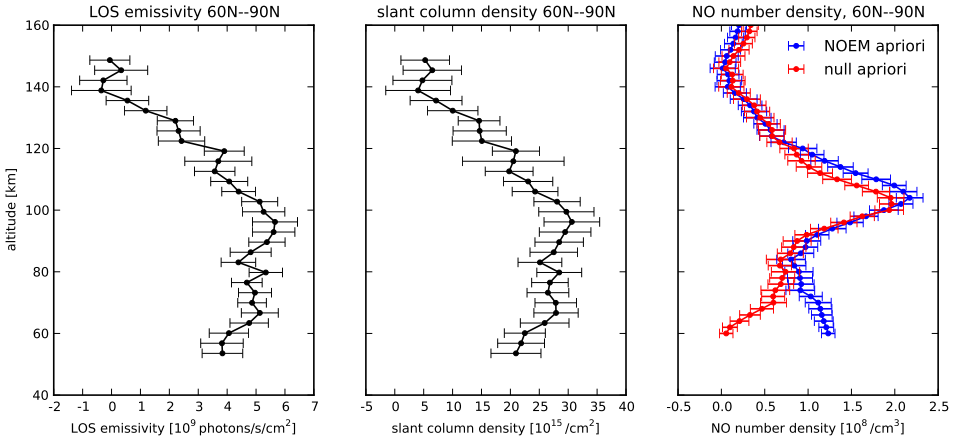

Fig. 4. Zonal mean (60° N–90° N) integrated NO emissivity profile (3 February 2010) (left panel), zonal mean fitted slant column densities (middle panel), and zonal mean NO number densities (right panel) using the NOEM model as a priori input (blue line) and without prior assumptions (red line). The error bars show the 3σ confidence interval.

AMTD
6, 3611–3642, 2013

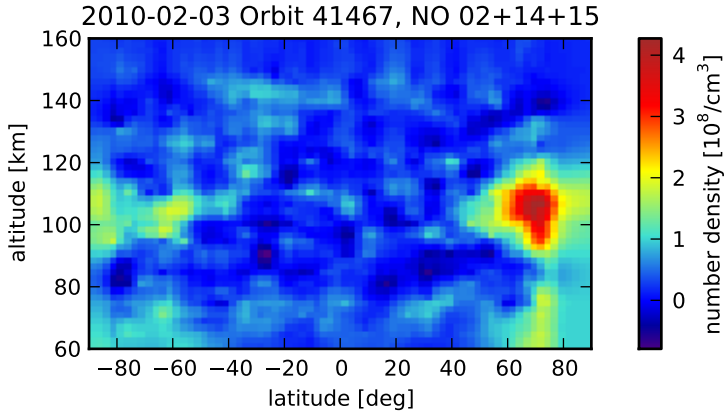

Fig. 5. Retrieved NO number densities along the sample orbit (no. 41467, 3 February 2010).

AMTD
6, 3611–3642, 2013

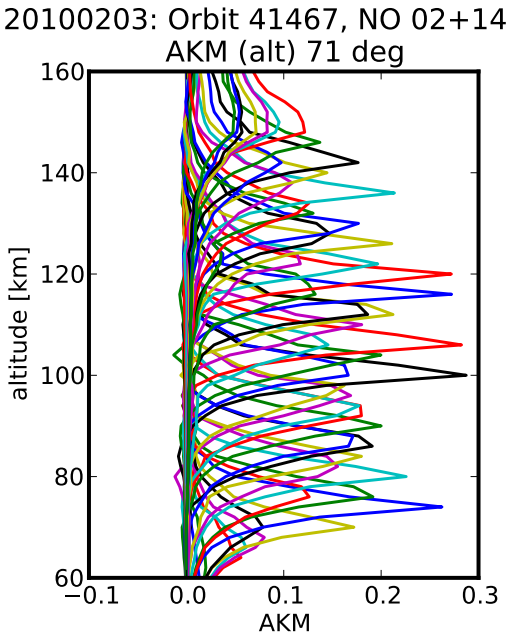

Fig. 6. Altitude averaging kernel matrix elements for a sample orbit (no. 41467, 3 February 2010).

AMTD
6, 3611–3642, 2013

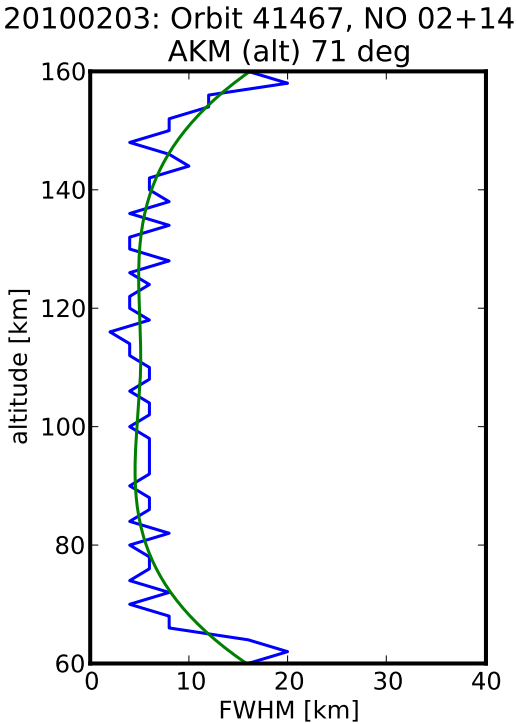

Fig. 7. FWHM of the altitude averaging kernel matrix elements for a sample orbit (no. 41467, 3 February 2010) as an indicator of vertical resolution.

AMTD
6, 3611–3642, 2013

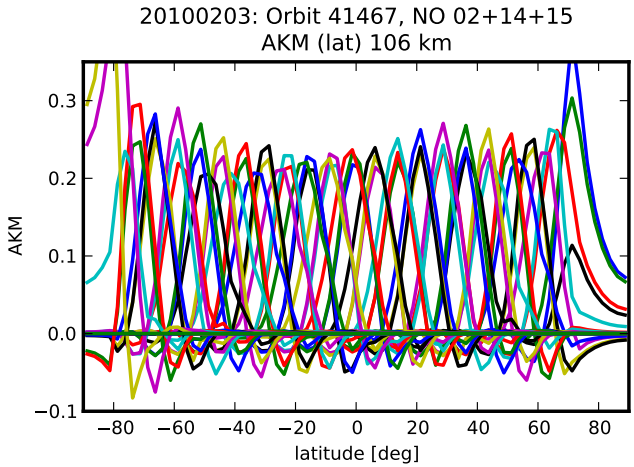

Fig. 8. Latitude averaging kernel matrix elements for a sample orbit (no. 41467, 3 February 2010).

AMTD
6, 3611–3642, 2013

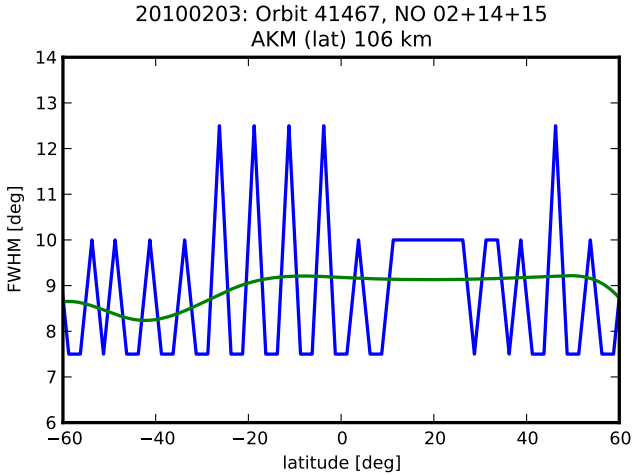

Fig. 9. FWHM of the latitude averaging kernel matrix elements for a sample orbit (no. 41467, 3 February 2010), indicating an average latitudinal resolution of about 9°.

AMTD
6, 3611–3642, 2013

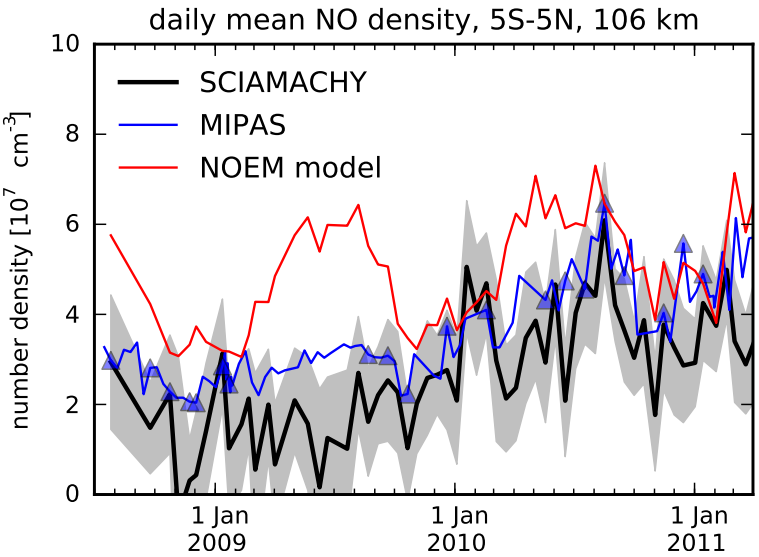

Fig. 10. Equatorial daily mean nitric oxide number density at 106 km, SCIAMACHY MLT (black) and MIPAS UA (blue) compared to the NOEM model (red) (Marsh et al., 2004) based on SNOE data (Barth et al., 2003). The grey shaded area shows the 3σ confidence interval of the SCIAMACHY daily means and the blue triangles indicate coincident SCIAMACHY MLT and MIPAS UA measurement days.

AMTD
6, 3611–3642, 2013

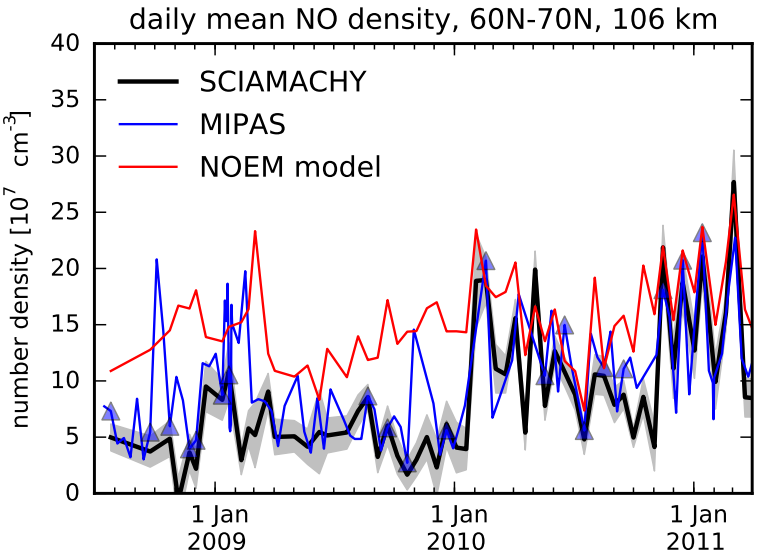

Fig. 11. Auroral daily mean nitric oxide number density at 106 km, SCIAMACHY MLT (black) and MIPAS UA (blue) compared to the NOEM model (red) (Marsh et al., 2004) based on SNOE data (Barth et al., 2003). The grey shaded area shows the 3σ confidence interval of the SCIAMACHY daily means and the blue triangles indicate coincident SCIAMACHY MLT and MIPAS UA measurement days.

AMTD
6, 3611–3642, 2013

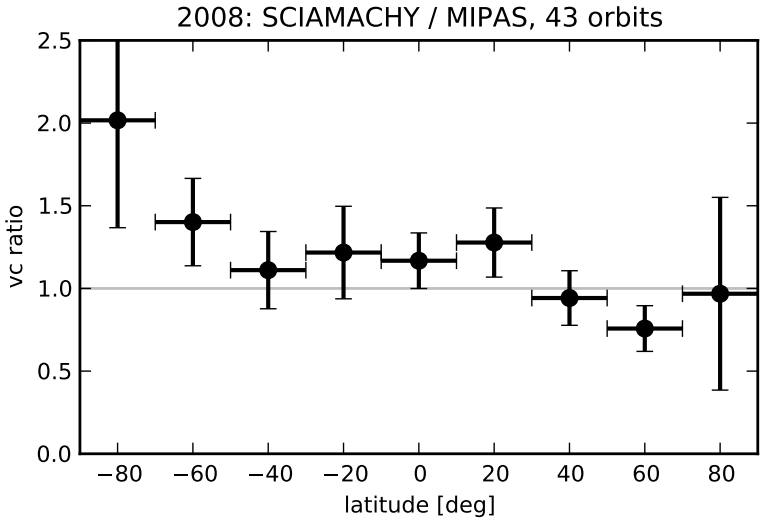

Fig. 12. Ratio of SCIAMACHY to MIPAS NO vertical columns (70–140 km), averaged in 20° latitude bins from 43 coincidence orbits in 2008. The horizontal bars indicate the bins and the vertical bars the 3σ confidence interval.

AMTD
6, 3611–3642, 2013

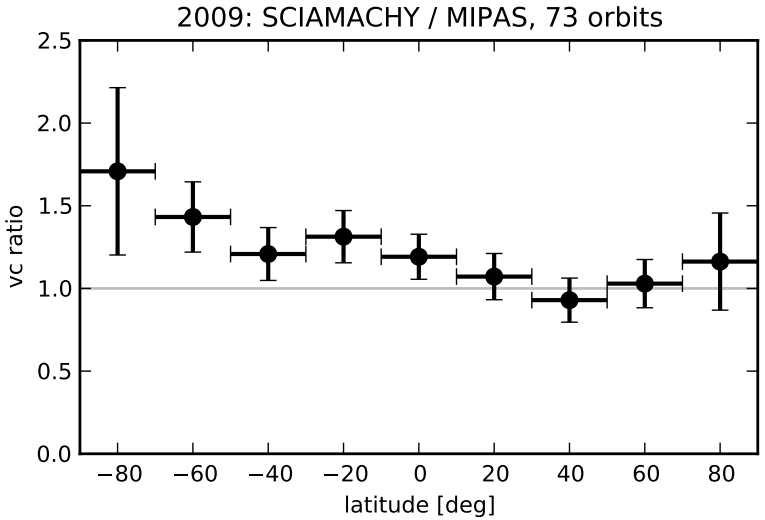

Fig. 13. Ratio of SCIAMACHY to MIPAS NO vertical columns (70–140 km), averaged in 20° latitude bins from 73 coincidence orbits in 2009. The horizontal bars indicate the bins and the vertical bars the 3σ confidence interval.

AMTD
6, 3611–3642, 2013